PROCEEDINGS OF SPIE

SPIEDigitalLibrary.org/conference-proceedings-of-spie

Brillouin optical time domain analysis with dual-frequency self-injection locked DFB laser

Cesar Lopez-Mercado, Pavel Itrin, Dmitry Korobko, Igor Zolotovskii, Andrei Fotiadi

Cesar Lopez-Mercado, Pavel Itrin, Dmitry A. Korobko, Igor O. Zolotovskii, Andrei A. Fotiadi, "Brillouin optical time domain analysis with dual-frequency self-injection locked DFB laser," Proc. SPIE 12139, Optical Sensing and Detection VII, 121391D (17 May 2022); doi: 10.1117/12.2621130

SPIE.

Event: SPIE Photonics Europe, 2022, Strasbourg, France

Brillouin Optical Time Domain Analysis with Dual-Frequency Self-Injection Locked DFB Laser

C. A. Lopez-Mercado[a], P. A. Itrin[b], D. A. Korobko[b], I. O. Zolotovskii[b], A. A. Fotiadi[b,c,d]
[a]Centro de Investigación Científica y de Educación Superior de Ensenada,
Carretera Ensenada-Tijuana No.3918, Zona Playitas, 22860 Ensenada, B.C., Mexico.
[b]Ulyanovsk State University, 42 Leo Tolstoy Street, Ulyanovsk, 432970, Russia.
[c]Ioffe Physico-Technical Institute of the RAS, 26 Polytekhnicheskaya Street,
St. Petersburg 194021, Russia.
[d]University of Mons, Boulevard Dolez 31, 7000 Mons, Belgium.

ABSTRACT

Self-injection locking to an external fiber cavity is an efficient technique enabling drastic linewidth narrowing of semiconductor lasers. Recently, we have introduced a simple dual-frequency laser source that employs self-injection locking of a DFB laser in the external ring fiber cavity and Brillouin lasing in the same cavity. The laser performance characteristics are on the level of the laser modules commonly used with Brillouin Optical Time Domain Analysis (BOTDA). The use of a laser source operating two frequencies strongly locked through the Brillouin resonance simplifies the BOTDA system, avoiding the use of a broadband electrooptical modulator (EOM) and high-frequency electronics. In this work, in a direct comparison with the commercial BOTDA, we explore the capacity of our low-cost solution for BOTDA sensing, demonstrating distributed measurements of the Brillouin frequency shift in a 10 km sensing fiber with a 1.5 m spatial resolution.

Keywords: Brillouin distributed sensing; self-injection locking; fiber ring cavity; Brillouin lasers.

1. INTRODUCTION

Distributed optical fiber sensors show superior advantages over their electronic counterparts due to their high sensitivity to external disturbances and low loss transmission important for remote sensing[1]. Unlike single-point optical fiber sensors[2-7] distributed optical fiber sensors[8] could interrogate and spatially resolve measurands along an unperturbated optical fiber, due to their specific sensing mechanisms[9-14]. Among them Brillouin-based distributed sensors[15-17] have attracted immense interest in recent years in fields like health monitoring of large structures in oil and gas pipelines[18], railways and high voltage transmission lines[19], high temperature distributed measurement in industrial applications[20], distributed strain measurement for cracks detection[21] and structural health monitoring[22]. The conventional distributed Brillouin optical fiber sensing is based on the backward stimulated Brillouin scattering, where the strain or temperature is a linear function of the Brillouin frequency shift (BFS) and so can be recovered from the distribution of Brillouin gain spectra (BGS) along the sensing fiber[23, 24]. Over the past two decades, many efforts have been made to improve its performances, including spatial resolution, measurement time, and sensing range[25-27]. Although the Brillouin sensing instruments have become commercially available, a relatively high cost remains the major critical factor limiting the range of their potential applications. A key and most expensive part of the traditional BOTDA system is a master-oscillator module employed for generation and tuning of the pump and Stokes signal frequencies. Commonly such module implements Phase-Locked Loop (PLL)[28] or optical side-band (OSB) generation techniques[29]. In PLL technique, two narrowband laser sources are used to generate pump and Stokes laser frequencies. The frequency of one laser is locked to the frequency of the second laser through a feedback circuit which allows tuning the frequency difference. This technique requires the use of a high-frequency photodetectors and RF-generators. In OSB method, only one narrowband laser is used, whereas the second frequency is generated through a broadband electro-optical modulator (EOM) driven at the frequency corresponding to the desired frequency shift (~11 GHz). This technique employs a broadband EOM and high-frequency drivers. Therefore, besides the narrowband laser sources with stricken requirements to stability, both methods require the use of rather costly high-frequency devices and electronic circuits. Considerable efforts have been

Optical Sensing and Detection VII, edited by Francis Berghmans, Ioanna Zergioti, Proc. of SPIE
Vol. 12139, 121391D · © 2022 SPIE · 0277-786X · doi: 10.1117/12.2621130

addressed to simplify the generation and tuning of pump and Stokes signals. A number of new BOTDA solutions have been proposed. Among them are sensors employing a single optical source driven by a pulsed RF signals and passive optical filtering[30], systems based on time-division pump-probe generation by direct modulation of a laser diode through an arbitrary waveform generator[31] and sources which use the Stokes wave generated inside a highly nonlinear fiber[32]. The idea to use a stabilized Brillouin fiber laser has been raised and investigated for this purpose[33-35]. However, the stabile lasers have been supplied by rather expensive active stabilization circuits. Concerning the capacity of BOTDA systems based on Brillouin laser sources, the previous works have not been conclusive and no comparison with the commercial BOTDA systems has been demonstrated.

An alternative solution for the dual-frequency laser potentially suitable for BOTDA applications has been reported recently[36, 37]. The principle of the laser operation is based on the self-injection locking mechanism that enables the reduction of a DFB laser linewidth down to sub-kHz[38, 39]. The ability of this low-cost source to replace the standard laser in the phase-OTDR analyzer has been experimentally demonstrated[40, 41]. In the dual-frequency laser configuration [42], the same ring fiber cavity is used to generate narrow-band coherent light at the pump frequency (through self-injection locking mechanism) and narrow-band coherent light at Stokes frequency (through stimulated Brillouin scattering). The laser is supplied by a simple low-bandwidth active optoelectronic feedback circuit governed by a low-cost USB-DAQ card [43]. Importantly, the drastic narrowing of the DFB laser linewidth to the sub-kHz range is provided by the self-injection-locking mechanism, whereas the active feedback is used only to maintain the laser operation in this regime. Therefore, in terms of feedback circuit bandwidth, complexity, and allocated memory, this method is much less consuming than the optoelectronic systems commonly used with Brillouin fiber lasers, including the lasers reported early for BOTDA sensing[34].

In this paper, we explore the potential of this low-cost laser solution for operation with Brillouin Optical Time Domain Analyzer (BOTDA)[24]. We present an extended description of the experimental results evaluating the capacity of the reported laser configuration for distributed measurements of the Brillouin frequency shift (BFS) in a 10-km fiber testing line with a spatial resolution of 1.5 m. The control measurements in the same testing line have been performed with a commercial BOTDA (OZ-optics, Inc.) set to interrogate with the same spatial resolution. A direct comparison of the results highlights no deterioration of the BOTDA system characteristics associated with the use of low-cost dual-frequency laser. Importantly, the laser source operating two frequencies strongly locked through the Brillouin resonance simplifies the BOTDA system and excludes the use of a broadband EOM, and high-frequency electronics commonly employed with the BOTDA system based on a single master-oscillator.

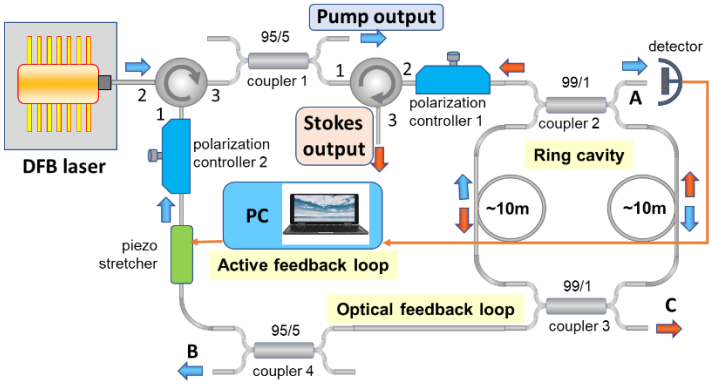

Figure 1. Dual-frequency laser sources used as the master-oscillator in BOTDA setup.

2. DUAL-FREQUENCY LASER

We have evaluated the performance of a BOTDA system using the low-cost self-injection locked DFB laser as a dual-frequency master oscillator[44]. A simple laser configuration is spliced from standard telecom components. It employs a single DFB laser coupled to an all-fiber ring cavity. In this configuration, the same ring fiber cavity is used both for self-injection locking of the DFB laser and for generation of Stokes light through the Brillouin lasing. A low-cost USB-DAQ is used to stabilize the system preventing mode-hopping. Specifically, a narrowband laser operation is provided by the self-injection locking mechanism, whereas the active feedback circuit just helps the laser maintain the desired operation. Additionally, the self-injection locking supports permanent coupling between the DFB laser and

external fiber ring cavity enabling an efficient resonant pumping for the low-noise Brillouin wave generation. The ability to emit light from a single DFB laser at two frequencies strongly locked to the Brillouin resonance has significantly simplified the traditional BOTDA setup, in particular, avoiding the use of broadband electrooptical modulators and related electronic circuits.

The experimental configuration of dual-frequency laser is shown in Fig. 1. The semiconductor laser is a commercial distributed feedback (DFB) laser diode (MITSUBISHI FU-68PDF-V520M27B) delivering ~15 mW at ~1535 nm. It is assembled within a standard 14-pin butterfly package. The DFB laser is coupled to the fiber ring cavity through a circulator. The high-Q external ring cavity is spliced from two (99/1) couplers. Totally, it comprises 20-m length of SMS-28 fiber (Corning, Inc.) perfectly adjusted for lasing at the Stokes Brillouin frequency[45]. To implement the self-injection locking, the first coupler provides passive feedback to the laser operation redirecting a part of the light circulating clockwise (CW) inside the cavity through the circulator back into the DFB laser cavity. The polarization controller 1 is used to adjust the polarization state of the light inside the fiber ring cavity enabling an optimal coupling between the laser radiation and one of the ring cavity modes. The polarization controller 2 adjusts the polarization state of the light before its injection into the DFB laser emitting a linear polarization thus controlling the optical feedback strength. A piezo fiber stretcher (PFS, Evanescent Optics Inc., Model 915B) is attached to the feedback loop. It is used as an optical phase shitter driven by a low-cost USB Multifunction DAQ (National Instrument NI USB-6009). The DAQ is connected with a PC and helps the laser maintain the desired operation in self-injection locking regime. The fiber configuration is spliced from standard telecom components and placed into a foam box stabilized at ~ 25°C thus protecting the laser system from the laboratory environment. A fast photodetector detects the optical signal at port A that is used as an error signal for operation of the active feedback circuit. The active feedback circuit tends to keep it as low as possible providing an appropriate voltage to the piezo fiber stretcher. Additional thermal control is applied to the laser box as a whole and used to keep the voltage applied to the piezo-stretcher within its dynamical range.

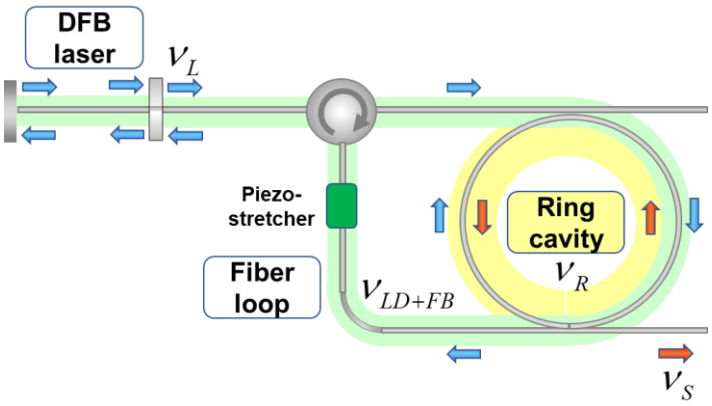

Figure 2. Dual-frequency laser operation: green background shows the coupled cavity comprising the DFB laser and feedback loop, yellow background marks the ring cavity.

The mechanism of the laser operation and stabilization has been discussed in[42, 43, 46, 47]. A simplified view on the laser operation is depicted in Fig. 2. The light emitted by a DFB laser passes the fiber ring cavity and optical feedback loop and is injected back into the DFB laser cavity forcing the DFB laser to emit at $\nu_L = \nu_R$, where ν_R is one of the ring cavity resonant frequencies. For stable laser operation, the laser frequency ν_L should be also resonant for the coupled cavity comprising the DFB laser cavity and feedback loop ν_{FB+LD}, so $\nu_L = \nu_R = \nu_{LD+FB}$. The position of the frequency ν_{LD+FB} in respect to ν_R is controlled by the piezo-stretcher through the applied voltage. The laser operation becomes unstable when the environment noise affecting the laser configuration fibers violates the equality $\nu_R = \nu_{LD+FB}$. The task addressed to the active feedback circuit is to maintain the equality $\nu_R = \nu_{LD+FB}$ minimizing the error signal detected at port A. In this case, the laser power at $\nu_L = \nu_R$ is perfectly coupled to the fiber ring cavity and enables effective backward lasing at Stokes frequency $\nu_S = \nu_L - \Delta_{SBS}$, where Δ_{SBS} is the Brillouin frequency shift. With the well-adjusted fiber ring cavity length, the Stokes frequency coincides with one of the resonant ring resonances. Therefore, a perfect stabilization of the lasing at $\nu_L = \nu_R = \nu_{LD+FB}$ ensures stabilization of lasing at the frequency ν_S.

In accordance with our observations, there are two cases when mode-hopping in the laser occurs. First, it is a mechanical vibration like a pencil kick on the laser box that causes short-time perturbations of the laser power (see, Fig. 5). We use a form box to protect the laser from mechanical vibrations. Second, it is an extended temperature drift. While the active feedback circuit operates against the temperature drift, the voltage applied to the piezo-stretcher could exhaust its dynamic range ($\pm 20\ rad$). In this case, for further operation, the phase delay induced by the piezo-stretcher should be reset by an integer number of 2π. Such a jump destabilizes the laser in the same way as the pencil kick does. To avoid the destabilization, the working point of the piezo-stretcher should be always maintained within its dynamical range. In our setup it is implemented through the additional thermal control applied to the laser box and using the voltage applied to the piezo-stretcher as an error signal.

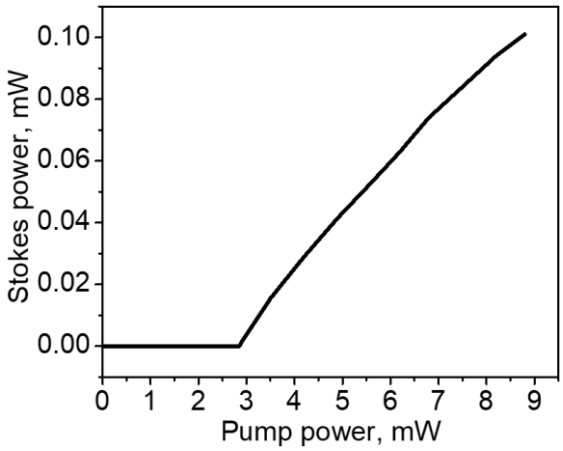

Figure 3. Stokes output power as a function of the pump output power.

The maximal laser output powers emitted by the laser are $\sim 9\ mW$ and $\sim 100\ \mu W$ for the pump and Stokes laser outputs, respectively. The experimental dependence of the laser power at the Stokes frequency (Stokes output) on the laser power at the pump frequency (Pump output) is shown in Fig. 3. The pump power threshold for the Stokes frequency generation is ~2.9 mW. The pump-to-Stokes power conversion efficiency above the threshold is ~3.3%. The laser optical spectra recorded with pump and Stokes laser outputs are shown in Fig.4. The spectra are centered at 1531.13 nm and 1531.21 nm, respectively. The difference of ~0.08 nm in the peak wavelengths corresponds to the Brillouin frequency shift (BFS) of ~11 GHz.

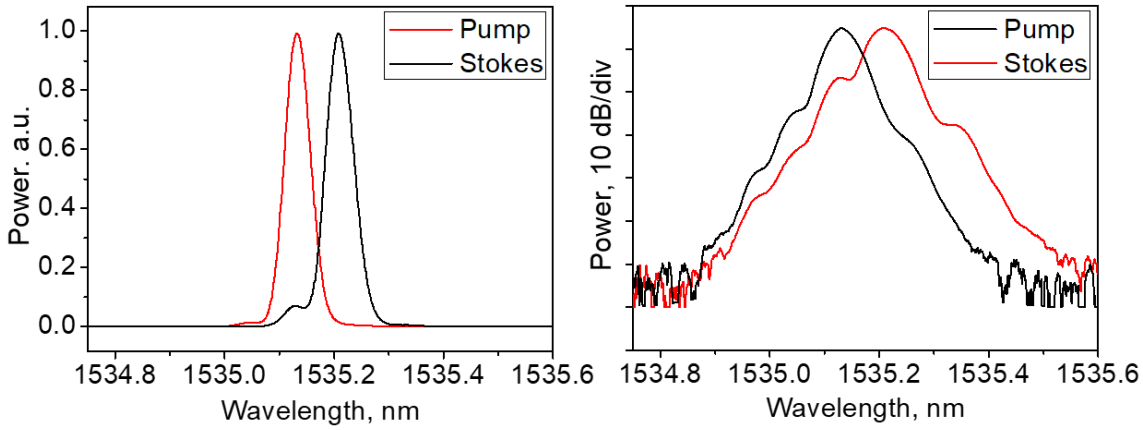

Figure 4. Typical RF beat spectrum measured with two master-oscillator outputs in (a) linear and (b) dB scales.

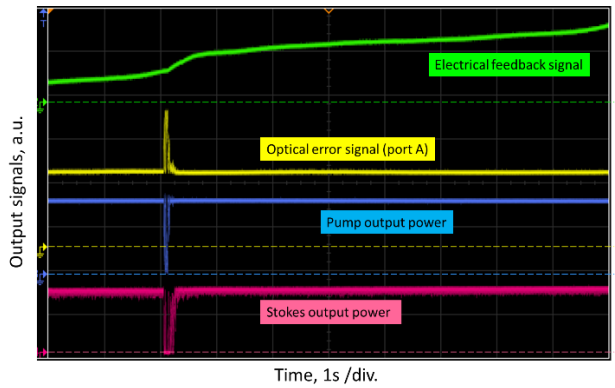

Figure 5. Typical oscilloscope traces of the optical error signal (port A), pump and Stokes output powers and electrical feedback signal highlighting the response on a knock on the fiber ring.

The typical laser oscilloscope traces recorded at pump output, Stokes output, optical error signal (port A), and the electrical feedback signal are shown in Fig. 5. The recorded traces give insight into the system stability demonstrating system response to a pencil kick on the spliced fiber setup. Due to the active feedback circuit, the power at port A (used as the error signal) always tends to its minimal value thus enabling a stable laser operation at two frequencies. All unperturbed optical power traces are almost flat and exhibit no fluctuations. When the configuration is perturbed by the pencil kick, the traces exhibit a dynamical behavior. The optical error signal makes a few stochastic fluctuations and then stabilizes to the original level. The time constants of the feedback mechanism are $\tau_L \sim 0.2\,s$ and $\tau_S \sim 0.05\,s$ for the pump and Stokes outputs, respectively. The degree of polarization measured by the polarization analyzer (HP 8509A\B) are ~ 100% for the pump and Stokes laser outputs.

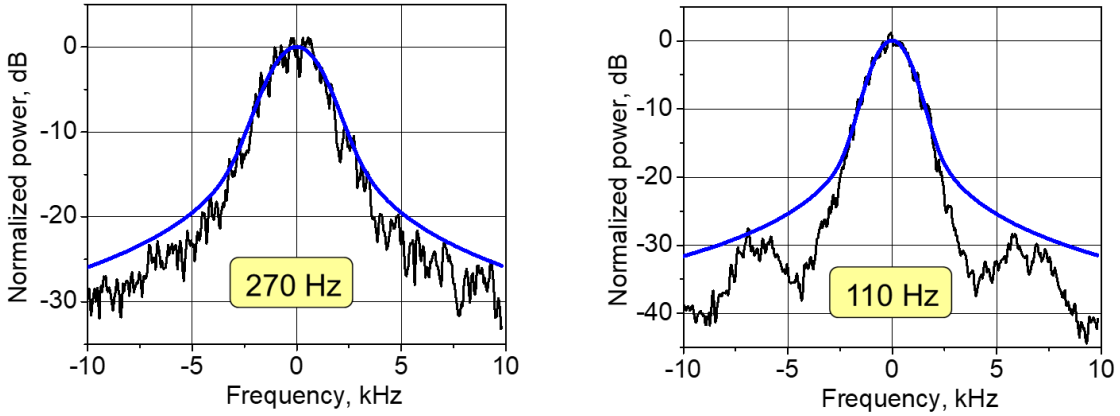

Figure 6. The self-heterodyne spectra of the pump (a) and Stokes (b) laser radiation. The measured spectra (black) and their fitting by the Voigt functions (blue). The fitting parameters evaluating the Gaussian and Lorentzian contributions are $w_G = 2.2kHz$, $w_L = 540Hz$ and $w_G = 1.7kHz$, $w_L = 220Hz$, for the pump and Stokes outputs, respectively.

The self-heterodyne spectra[48, 49] of the pump (a) and Stokes (b) laser radiation averaged over 10 realizations each are shown in Fig. 6. The measurements have been performed with the fiber Mach–Zehnder interferometer (comprising the 55 km delay fiber and 25 MHz phase modulator), ~5 GHz photodetector, and RF spectrum analyzer (FSH8, Rohde & Schwarz). The recorded spectra are fitted by the Voigt profile and decomposed into the Gaussian and Lorentzian contributions[49, 50]. The fitting parameter w_L relates to the laser Lorentzian linewidth as $1/2\,w_L$ resulting in the measured values of $\sim 270Hz$ and $\sim 110Hz$ for pump and Stokes laser outputs, respectively[49].

The power spectral density (PSD) of phase noise measured for the pump and Stokes radiations with a RF spectrum analyzer (Agilent N9320A) in the range of $10-100\,kHz$ is shown in Fig. 7 (a). The measurements have been performed by the self-heterodyne method[51-53] with the Mach–Zehnder interferometer comprising the $\sim 1.3\,km$ delay fiber

($\sim 5.76\ \mu s$) and $20\ MHz$ frequency modulator. In comparison with the free-running laser the measured PSD is lower by $\sim(35-40)$ and $\sim(50-60)\ dBc/Hz$ for the pump and Stokes laser outputs, respectively. The relative intensity noise (RIN) measured with a lock-in amplifier SRS510 in the range of $1-100\ kHz$ is shown in Fig. 7 (b). In comparison with the free-running laser the measured RIN is lower by $\sim(5-10)\ dB$ and higher by $30-40\ dB$ for the pump and Stokes laser outputs, respectively.

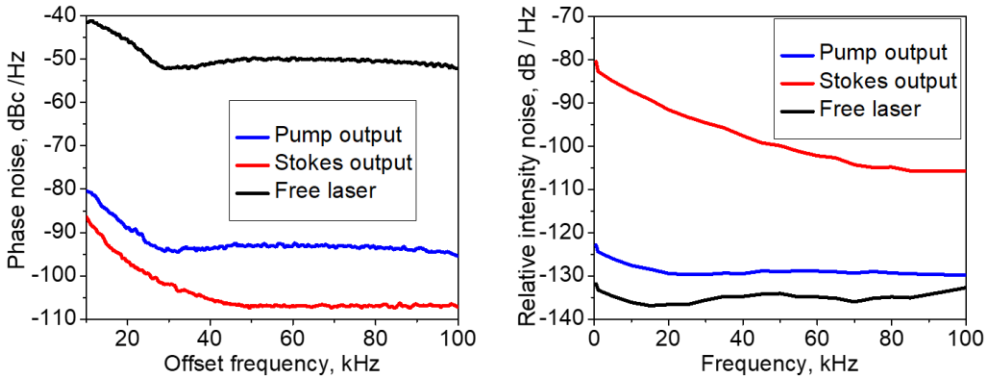

Figure 7. Noise performance of the laser. (a) Phase noise; (b) Relative Intensity noise (RIN)

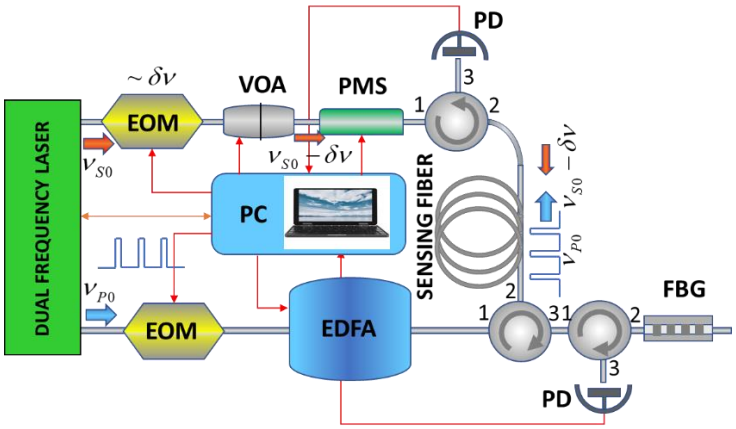

Figure 8. The experimental BOTDA setup.

3. BRILLOUIN OPTICAL TIME DOMAIN ANALYSER (BOTDA) SETUP

Our experimental BOTDA configuration is shown in Fig. 8. A simple self-injection locked Brillouin laser operating at 1535 nm[42] is used as a master oscillator. The laser generates two monochromatic optical waves at pump (ν_{L0}) and Stokes (ν_{S0}) frequencies delivered through two independent fiber outputs. The laser operation is characterized by natural Lorenz linewidths of ~270 Hz and ~110 Hz and powers of $\sim 9\ mW$ and $\sim 100\ \mu W$ for pump and Stokes outputs, respectively. The laser optical spectra shown in Fig. 3 demonstrate the contrast of ~70 dB between the peak and background powers for both laser outputs. The beating between two laser outputs is characterized by a stable radio-frequency (RF) spectrum with 290-Hz-linewidth and fixed peak frequency at $\Delta\nu_0 = \nu_{L0} - \nu_{S0} \sim 10.950\ GHz$ presented in Fig. 9 (a). To reduce the effect of the environment noise, the spliced laser configuration is placed into a thermostabilized (~ 25°C) foam box. Additional thermal control is applied to the laser box as a whole and used to keep the feedback circuit within its dynamical range, ensuring long-term laser operation stability. The drift of the RF beating frequency recorded each minute for 1 hour is shown in Fig. 9 (b).

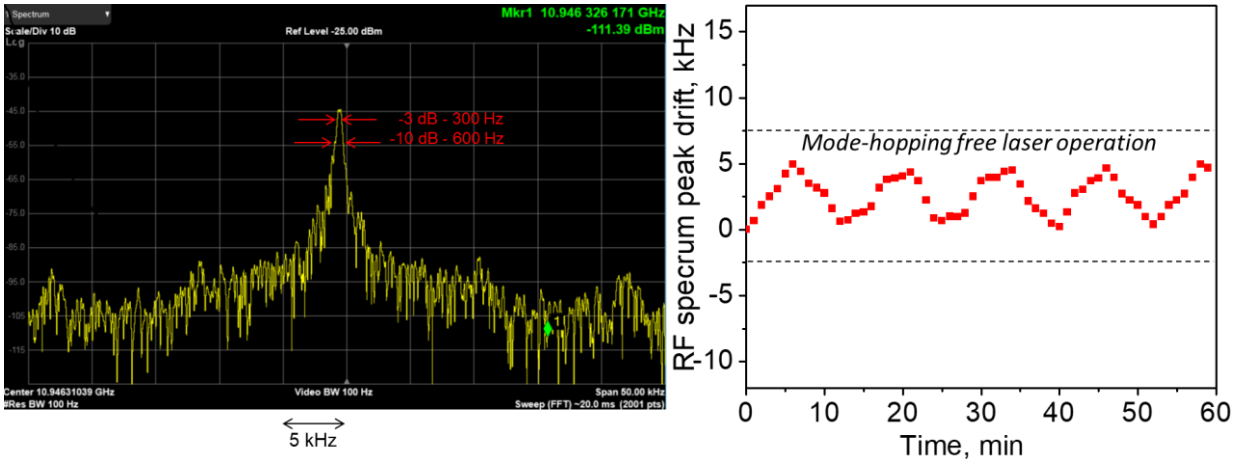

Figure 9. (a) Typical RF beat spectrum measured with two master-oscillator outputs. (b) Drift of the RF beat spectrum peak frequency measured each minute for 60 minutes.

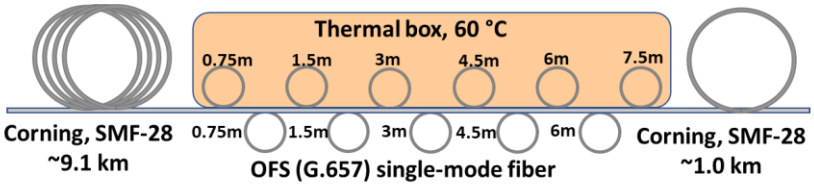

Figure 10. Optical fiber line for BOTDA testing

The BOTDA built in the lab is a simple modification of the traditional pump - probe setup [54]. The laser radiation at the pump frequency ν_{L0} passes through the electro-optical intensity modulator (EOM 1) and erbium-doped fiber amplifier (EDFA) to form a periodic train of rectangular pulses with the peak power of ~300 mW, pulse duration of ~15 ns and repetition rate of ~10 kHz. The laser radiation emitted at the Stokes frequency ν_{S0} passes through the dual-drive electro-optic modulator (EOM 2, SSB-CS EOM, Sumitomo), variable optical attenuator (VOA) and polarization mode scrambler (PMS) to form a ~10μW CW probe signal at the frequency $\nu_S = \nu_{S0} - \delta\nu_S$. The frequency tuning of the probe signal is provided by a tunable radio-frequency generator supplying EOM 2 at $\delta\nu_S < 1GHz$. The pump pulses at ν_{L0} and CW probe signal at ν_S are introduced into the fiber under test from opposite fiber ends. Their interaction through the Brillouin process in the fiber under test causes an energy transfer from the pump pulse to the CW Stokes signal leading to its intensity modulation recorded at the fiber output by the fast photodetector and PC acquisition card. The modulation amplitude (typically <100nW) of the probe signal is proportional to the local Brillouin gain at the fiber point, where Brillouin resonance is achieved. The recorded probe signal traces are averaged over 4096 pump pulses and used to map distribution of the Brillouin gain over the fiber length. The traces recorded at different $\delta\nu_S$ are used to build the Brillouin gain spectrum at each fiber point. Then, these data are mathematically processed to find the position of the Brillouin spectrum peak, i.e., the BFS, in each fiber point. The pump pulse duration of ~15 ns sets the system spatial resolution of ~1.5m. It is worth noting that the use of the laser source operating two frequencies strongly locked through the Brillouin resonance as a master-oscillator in our BOTDA setup has allowed replacing the broadband EOM used in [54] for the frequency shift by ~11 GHz and all supplying high-frequency electronics by more cost-efficient and straightforward counterparts operating in sub-GHz radio-frequency range.

To evaluate the performance of the laser operation with the built BOTDA, we have collected a fiber testing line similar to that commonly used with BOTDAs for their calibration. The 10-km-length testing line shown in Fig. 10 comprises two lengths of SMF-28 Corning fiber (9.1 km and 1 km) and a length of OFS (G.657) fiber (~50 m) placed between them. The latter includes eleven altered fiber coils of different lengths (0.75-6.0 m) kept at different temperatures. Odd coils are placed into a heat chamber thermostabilized at 60 ºC, while even coils are rested at room temperature (~25 ºC). The measured distribution of the BFS over the OFS fiber follows the temperature fiber profile with the factor of ~1 MHz/°C.

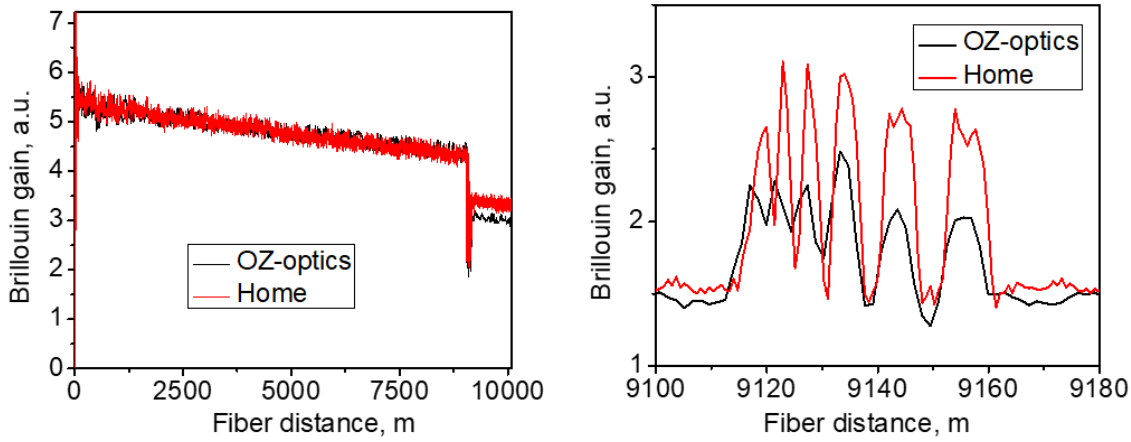

Figure 11. The measured distribution of the Brillouin gain (a) over the whole testing line and (b) over the range of 9.1 - 9.18 km.

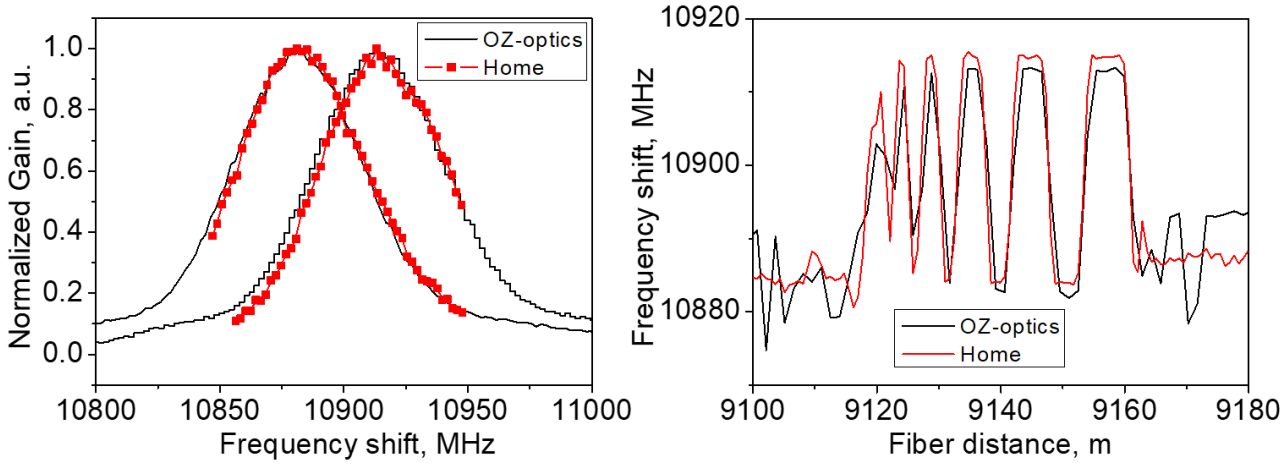

Figure 12. The Brillouin gain spectra (BGS) measured in the fiber points of 9151 m and 9157 m exposed to the temperature of ~25 ºC and ~60 ºC, respectively; (b) the measured distribution of the Brillouin frequency shift (BFS) over the range of 9.1 - 9.18 km

4. RESULTS OF BOTDA TESTING

The testing experiments have been performed with our BOTDA setup and then repeated with the commercial BOTDA system (OZ-optics) set to operate with the pump pulse of 15 ns. Note, the operating wavelength of the commercial BOTDA is 1550 nm, so the BFS data measured with this device are presented here with the scaling factor of 1550/1535. The experimental results are shown in Fig. 11 and 12. First, we have adjusted the frequency difference between the pump and probe signal $\Delta\nu_0 + \delta\nu_S$ to maximize the signal recorded from the first length of the SMS-28 fiber. In this case, $\delta\nu_S \approx 0$, since the frequency difference of two signals emitted by the laser corresponds to the BFS in the SMS-28 fiber at room temperature ($\sim 10.946\,GHz$). Fig. 11 (a) compares the traces recorded with our setup and the commercial BOTDA. One can see that both traces exhibit similar behavior, including the gain modulation pronounced in the fiber points with an alternating temperature. The drop of both traces after 9.2 km is explained by pump power loss after splicing. Fig. 11 (b) shows more details of the Brillouin gain modulation relating to the OFS fiber. Both systems well recognize the fiber segments, where the fiber temperature is higher than the room temperature. Since the BFS increases with the temperature, the BFS in hot OFS fiber segments is closer to the frequency difference set by the system leading to an increase of the local Brillouin gain measured in these points.

In order to accurately estimate the BFS distribution along the sensing fiber, the Brillouin gain spectrum (BGS) has been measured at each fiber location. At each fiber point, the radio-frequency $\delta\nu_S$ applied to the dual-drive EOM 2 has

been swept within the range of 100 MHz with a step of ~2 MHz. Then the BFS is reconstracted by fitting the recorded data with the Lorentzian profile[24]. Fig. 12 (a) compares the BGSs at two OFS fiber points located at 9151 m and 9057 m measured with our setup and the commercial BOTDA. One can see that our system well reproduces the BGS shape recorded with the commercial BOTDA. It is worth noting that the BGS corresponting to the fiber points exposed to the temperature ~25 ºC and ~60 ºC are shifted each to other by 35 MHz. Fig. 12 (b) shows the distributions of the BFS over the OFS fiber. One can see that the quality of BSF restoration is rather high. For the fiber segments longer than 1.5m both devices give almost the same distribution providing a good agreement in absolute peak frequencies varying from 10880 GHz (at ~25 ºC) to 10915 GHz (at ~60 ºC), resolved slopes and segment positions. All specific fiber segments are well recognized. For the fiber segment shorter than 1.5m our experimental device demonstrates even better accuracy than the commercial BOTDA operating with the same pulse duration.

5. CONCLUSIONS

In conclusion, we have utilized a simple dual-frequency laser configuration to operate with BOTDA. The use of the laser operating two fixed frequencies significantly simplifies the BOTDA system and allows to exclude the broadband EOM (and high-power high-frequency microwave generator supplying the EOM) from the traditional BOTDA configuration based on a single narrowband laser source. These rather expensive devices constitute a significant part of the BOTDA system value. Instead, a dual drive EOM supplied by a standard 1-GHz radio-frequency generator have been employed in our home BOTDA setup. Under control of the commercial BOTDA, we have evaluated the capacity of the low-cost laser solution to operate with the BOTDA sensing demonstrating distributed measurements of the BFS in a 10-km sensing fiber with 1.5m spatial resolution. No deterioration of the system performance characteristics associated with the use of the dual-frequency laser has been found during the measurements. Further research will be directed to design and testing of new laser sources intendent for operation with fiber optic monitoring systems enabling interrogating optical signals with rather specific performance characteristics[55-69].

ACKNOWLEDGEMENTS

The work was supported by the Ministry of Higher Education and Science of the Russian Federation (Megagrant Program, project #075-15-2021-581) and the Russian Science Foundation (project 18-12-00457P). The work of P.A.I. was supported by the Russian Fund of Basic Research (20-32-90171). The construction of the home-made BOTDA system was supported by the Russian Fund of Basic Research (19-42-730009 p_a).

REFERENCES

[1] Lee, B., "Review of the present status of optical fiber sensors," Optical Fiber Technology **9**, 57-79 (2003).
[2] Ahsani, V., Ahmed, F., Jun, M. B., and Bradley, C., "Tapered fiber-optic mach-zehnder interferometer for ultra-high sensitivity measurement of refractive index," Sensors **19**, 1652 (2019).
[3] Fotiadi, A. A., Brambilla, G., Ernst, T., Slattery, S. A., and Nikogosyan, D. N., "Tpa-induced long-period gratings in a photonic crystal fiber: Inscription and temperature sensing properties," Journal of the Optical Society of America B: Optical Physics **24**, 1475-1481 (2007).
[4] Brambilla, G., Fotiadi, A. A., Slattery, S. A., and Nikogosyan, D. N., "Two-photon photochemical long-period grating fabrication in pure-fused-silica photonic crystal fiber," Optics Letters **31**, 2675 (2006).
[5] Caucheteur, C., Fotiadi, A., Megret, P., Slattery, S. A., and Nikogosyan, D. N., "Polarization properties of long-period gratings prepared by high-intensity femtosecond 352-nm pulses," IEEE Photonics Technology Letters **17**, 2346-2348 (2005).
[6] Faustov, A. V., Gusarov, A., Wuilpart, M., Fotiadi, A. A., Liokumovich, L. B., Zolotovskiy, I. O., Tomashuk, A. L., de Schoutheete, T., and Megret, P., "Comparison of gamma-radiation induced attenuation in al-doped, p-doped and ge-doped fibres for dosimetry," IEEE Transactions on Nuclear Science **60**, 2511-2517 (2013).
[7] Udd, E., Du, H. H., and Wang, A., "Fiber optic sensors and applications vi," in *Fiber Optic Sensors and Applications VI*(2009).
[8] Barrias, A., Casas, J. R., and Villalba, S., "A review of distributed optical fiber sensors for civil engineering applications," Sensors (Basel) **16** (2016).

[9] Zheng, H., Zhang, J., Guo, N., and Zhu, T., "Distributed optical fiber sensor for dynamic measurement," Journal of Lightwave Technology **39**, 3801-3811 (2021).
[10] Bao, X., Zhou, Z., and Wang, Y., "Review: Distributed time-domain sensors based on brillouin scattering and fwm enhanced sbs for temperature, strain and acoustic wave detection," PhotoniX **2**, 14 (2021).
[11] Faustov, A. V., Gusarov, A. V., Mégret, P., Wuilpart, M., Zhukov, A. V., Novikov, S. G., Svetukhin, V. V., and Fotiadi, A. A., "Application of phosphate doped fibers for ofdr dosimetry," Results in Physics **6**, 86-87 (2016).
[12] Ding, Z., Wang, C., Liu, K., Jiang, J., Yang, D., Pan, G., Pu, Z., and Liu, T., "Distributed optical fiber sensors based on optical frequency domain reflectometry: A review," Sensors (Basel) **18**, 1072 (2018).
[13] Gorshkov, B. G., Yüksel, K., Fotiadi, A. A., Wuilpart, M., Korobko, D. A., Zhirnov, A. A., Stepanov, K. V., Turov, A. T., Konstantinov, Y. A., and Lobach, I. A., "Scientific applications of distributed acoustic sensing: State-of-the-art review and perspective," Sensors **22**, 1033 (2022).
[14] Faustov, A. V., Gusarov, A. V., Mégret, P., Wuilpart, M., Zhukov, A. V., Novikov, S. G., Svetukhin, V. V., and Fotiadi, A. A., "The use of optical frequency-domain reflectometry in remote distributed measurements of the γ-radiation dose," Technical Physics Letters **41**, 414-417 (2015).
[15] Kurashima, T., Horiguchi, T., and Tateda, M., "Distributed-temperature sensing using stimulated brillouin scattering in optical silica fibers," Opt Lett **15**, 1038-1040 (1990).
[16] Fellay, A., Thévenaz, L., Facchini, M., Niklès, M., and Robert, P., "Distributed sensing using stimulated brillouin scattering: Towards ultimate resolution," in *12th International Conference on Optical Fiber Sensors*(Optical Society of America, Williamsburg, Virginia, 1997), p. OWD3.
[17] Bao, X., Webb, D. J., and Jackson, D. A., "22-km distributed temperature sensor using brillouin gain in an optical fiber," Optics Letters **18**, 552-554 (1993).
[18] Johny, J., Amos, S., and Prabhu, R., "Optical fibre-based sensors for oil and gas applications," Sensors **21**, 6047 (2021).
[19] Hsu, W.-K., Lee, Y.-L., and Kuan, T.-T., "Brillouin frequency shift sensing technology used in railway strain and temperature measurement," Applied Sciences **11**, 7101 (2021).
[20] Shen, J., Li, T., Zhu, H., Yang, C., and Zhang, K., "Sensing properties of fused silica single-mode optical fibers based on ppp-botda in high-temperature fields," Sensors (Basel) **19**, 5021 (2019).
[21] Zhang, D., Yang, Y., Xu, J., Ni, L., and Li, H., "Structural crack detection using dpp-botda and crack-induced features of the brillouin gain spectrum," Sensors (Basel) **20**, 6947 (2020).
[22] Bado, M. F., and Casas, J. R., "A review of recent distributed optical fiber sensors applications for civil engineering structural health monitoring," Sensors (Basel) **21**, 1818 (2021).
[23] Dong, Y., "High-performance distributed brillouin optical fiber sensing," Photonic Sensors **11**, 69-90 (2021).
[24] Soto, M. A., [Distributed brillouin sensing: Time-domain techniques], Springer, Singapore (2018).
[25] Wang, B., Dong, Y., Ba, D., and Bao, X., "High spatial resolution: An integrative review of its developments on the brillouin optical time- and correlation-domain analysis," Measurement Science and Technology **31**, 052001 (2020).
[26] Dominguez-Lopez, A., Soto, M. A., Martin-Lopez, S., Thevenaz, L., and Gonzalez-Herraez, M., "Resolving 1 million sensing points in an optimized differential time-domain brillouin sensor," Opt Lett **42**, 1903-1906 (2017).
[27] Zhou, D., Dong, Y., Wang, B., Pang, C., Ba, D., Zhang, H., Lu, Z., Li, H., and Bao, X., "Single-shot botda based on an optical chirp chain probe wave for distributed ultrafast measurement," Light: Science & Applications **7**, 32 (2018).
[28] Brown, A. W., Smith, J. P., Bao, X., Demerchant, M. D., and Bremner, T., "Brillouin scattering based distributed sensors for structural applications," Journal of Intelligent Material Systems and Structures **10**, 340-349 (2016).
[29] Nikles, M., Thevenaz, L., and Robert, P. A., "Simple distributed fiber sensor based on brillouin gain spectrum analysis," Opt Lett **21**, 758 (1996).
[30] Iribas, H., Urricelqui, J., Mariñelarena, J., Sagues, M., and Loayssa, A., "Cost-effective brillouin optical time-domain analysis sensor using a single optical source and passive optical filtering," Journal of Sensors **2016**, 1-7 (2016).
[31] Song, K. Y., and Yang, S., "Simplified brillouin optical time-domain sensor based on direct modulation of a laser diode," Opt Express **18**, 24012-24018 (2010).
[32] Bravo, M., Ullan, A., Zornoza, A., Loayssa, A., Lopez-Amo, M., and Lopez-Higuera, J. M., "Application of remote power-by-light switching in a simplified botda sensor network," Sensors (Basel) **13**, 17434-17444 (2013).
[33] Marini, D., Iuliano, M., Bastianini, F., and Bolognini, G., "Botda sensing employing a modified brillouin fiber laser probe source," Journal of Lightwave Technology **36**, 1131-1137 (2018).
[34] Rossi, L., Marini, D., Bastianini, F., and Bolognini, G., "Analysis of enhanced-performance fibre brillouin ring laser for brillouin sensing applications," Opt. Express **27**, 29448-29459 (2019).

[35] Rossi, L., Marini, D., Bastianini, F., and Bolognini, G., "Enhanced performance short cavity brillouin fiber ring laser for high-stability botda sensing," in *2020 IEEE SENSORS*(2020), pp. 1-4.
[36] Spirin, V. V., Lopez-Mercado, C. A., Mégret, P., Korobko, D. A., Zolotovskii, I. O., and Fotiadi, A. A., "Stabilizing brillouin fiber laser for applications in distributed botda sensing," SPIE Proceedings **11772**, 1177207 (2021).
[37] Lopez-Mercado, C. A., Korobko, D. A., Zolotovskii, I. O., and Fotiadi, A. A., "Application of dual-frequency self-injection locked dfb laser for brillouin optical time domain analysis," Sensors **21**, 6859 (2021).
[38] Bueno Escobedo, J. L., Spirin, V. V., López-Mercado, C. A., Mégret, P., Zolotovskii, I. O., and Fotiadi, A. A., "Self-injection locking of the dfb laser through an external ring fiber cavity: Polarization behavior," Results in Physics **6**, 59-60 (2016).
[39] Spirin, V. V., Castro, M., López-Mercado, C. A., Mégret, P., and Fotiadi, A. A., "Optical locking of two semiconductor lasers through high-order brillouin stokes components in optical fiber," Laser Physics **22**, 760-764 (2012).
[40] Bueno Escobedo, J. L., Spirin, V. V., López-Mercado, C. A., Márquez Lucero, A., Mégret, P., Zolotovskii, I. O., and Fotiadi, A. A., "Self-injection locking of the dfb laser through an external ring fiber cavity: Application for phase sensitive otdr acoustic sensor," Results in Physics **7**, 641-643 (2017).
[41] Bueno Escobedo, J. L., Jason, J., López-Mercado, C. A., Spirin, V. V., Wuilpart, M., Mégret, P., Korobko, D. A., Zolotovskiy, I. O., and Fotiadi, A. A., "Distributed measurements of vibration frequency using phase-otdr with a dfb laser self-stabilized through pm fiber ring cavity," Results in Physics **12**, 1840-1842 (2019).
[42] Spirin, V. V., Bueno Escobedo, J. L., Korobko, D. A., Mégret, P., and Fotiadi, A. A., "Dual-frequency laser comprising a single fiber ring cavity for self-injection locking of dfb laser diode and brillouin lasing," Opt. Express **28**, 37322-37333 (2020).
[43] Spirin, V. V., Bueno Escobedo, J. L., Korobko, D. A., Mégret, P., and Fotiadi, A. A., "Stabilizing dfb laser injection-locked to an external fiber-optic ring resonator," Opt. Express **28**, 478-484 (2020).
[44] Spirin, V. V., Bueno-Escopedo, J. L., Lopez-Mercado, C. A., Mégret, P., Korobko, D. A., Zolotovskii, I. O., and Fotiadi, A. A., "Dual-frequency narrowband cw fiber laser implementing self-injection locking of dfb laser diode and brillouin lasing in a single ring cavity," SPIE Proceedings **11770**, 117701K (2021).
[45] López-Mercado, C. A., Spirin, V. V., Kablukov, S. I., Zlobina, E. A., Zolotovskiy, I. O., Mégret, P., and Fotiadi, A. A., "Accuracy of single-cut adjustment technique for double resonant brillouin fiber lasers," Optical Fiber Technology **20**, 194-198 (2014).
[46] Korobko, D. A., Zolotovskii, I. O., Panajotov, K., Spirin, V. V., and Fotiadi, A. A., "Self-injection-locking linewidth narrowing in a semiconductor laser coupled to an external fiber-optic ring resonator," Optics Communications **405**, 253-258 (2017).
[47] Spirin, V. V., Bueno Escobedo, J. L., Miridonov, S. V., Maya Sánchez, M. C., López-Mercado, C. A., Korobko, D. A., Zolotovskii, I. O., and Fotiadi, A. A., "Sub-kilohertz brillouin fiber laser with stabilized self-injection locked dfb pump laser," Optics & Laser Technology **141**, 107156 (2021).
[48] Derickson, D., Hentschel, C., and Vobis, J., [Fiber optic test and measurement], Prentice Hall PTR New Jersey (1998).
[49] Mercer, L. B., "1 /f frequency noise effects on self-heterodyne linewidth measurements," IEEE Lightwave Technology **9**, 485-493 (1991).
[50] Chen, M., Meng, Z., Wang, J., and Chen, W., "Ultra-narrow linewidth measurement based on voigt profile fitting," Opt. Express **23**, 6803-6808 (2015).
[51] Camatel, S., and Ferrero, V., "Narrow linewidth cw laser phase noise characterization methods for coherent transmission system applications," Journal of Lightwave Technology **26**, 3048-3055 (2008).
[52] Llopis, O., Merrer, P. H., Brahimi, H., Saleh, K., and Lacroix, P., "Phase noise measurement of a narrow linewidth cw laser using delay line approaches," Optics Letters **36**, 2713-2715 (2011).
[53] Li, Y., Fu, Z., Zhu, L., Fang, J., Zhu, H., Zhong, J., Xu, P., Chen, X., Wang, J., and Zhan, M., "Laser frequency noise measurement using an envelope-ratio method based on a delayed self-heterodyne interferometer," Optics Communications **435**, 244-250 (2019).
[54] Stiller, B., Kudlinski, A., Lee, M. W., Bouwmans, G., Delque, M., Beugnot, J.-C., Maillotte, H., and Sylvestre, T., "Sbs mitigation in a microstructured optical fiber by periodically varying the core diameter," IEEE Photonics Technology Letters **24**, 667-669 (2012).
[55] Popov, S. M., Butov, O. V., Chamorovski, Y. K., Isaev, V. A., Mégret, P., Korobko, D. A., Zolotovskii, I. O., and Fotiadi, A. A., "Narrow linewidth short cavity brillouin random laser based on bragg grating array fiber and dynamical population inversion gratings," Results in Physics **9**, 806-808 (2018).

[56] Popov, S. M., Butov, O. V., Bazakutsa, A. P., Vyatkin, M. Y., Chamorovskii, Y. K., and Fotiadi, A. A., "Random lasing in a short er-doped artificial rayleigh fiber," Results in Physics **16**, 102868 (2020).
[57] Korobko, D. A., Zolotovskii, I. O., Svetukhin, V. V., Zhukov, A. V., Fomin, A. N., Borisova, C. V., and Fotiadi, A. A., "Detuning effects in brillouin ring microresonator laser," Opt Express **28**, 4962-4972 (2020).
[58] Phan Huy, K., Nguyen, A. T., Brainis, E., Haelterman, M., Emplit, P., Corbari, C., Canagasabey, A., Kazansky, P. G., Deparis, O., Fotiadi, A. A., Mégret, P., and Massar, S., "Photon pair source based on parametric fluorescence in periodically poled twin-hole silica fiber," Opt. Express **15**, 4419 (2007).
[59] Ribenek, V. A., Stoliarov, D. A., Korobko, D. A., and Fotiadi, A. A., "Pulse repetition rate tuning of a harmonically mode-locked ring fiber laser using resonant optical injection," Optics Letters **46**, 5687-5690 (2021).
[60] Ribenek, V. A., Stoliarov, D. A., Korobko, D. A., and Fotiadi, A. A., "Mitigation of the supermode noise in a harmonically mode-locked ring fiber laser using optical injection," Optics Letters **46**, 5747-5750 (2021).
[61] Kbashi, H. J., Sergeyev, S. V., Al-Araimi, M., Rozhin, A., Korobko, D., and Fotiadi, A., "High-frequency vector harmonic mode locking driven by acoustic resonances," Optics Letters **44**, 5112-5115 (2019).
[62] Lobach, I. A., Drobyshev, R. V., Fotiadi, A. A., Podivilov, E. V., Kablukov, S. I., and Babin, S. A., "Open-cavity fiber laser with distributed feedback based on externally or self-induced dynamic gratings," Optics Letters **42**, 4207 (2017).
[63] Korobko, D. A., Fotiadi, A. A., and Zolotovskii, I. O., "Mode-locking evolution in ring fiber lasers with tunable repetition rate," Opt. Express **25**, 21180 (2017).
[64] Lobach, I. A., Kablukov, S. I., Podivilov, E. V., Fotiadi, A. A., and Babin, S. A., "Fourier synthesis with single-mode pulses from a multimode laser," Optics Letters **40**, 3671 (2015).
[65] Fotiadi, A. A., Korobko, D. A., Zolotovskii, I. O., and Taylor, J. R., "Brillouin-like amplification in rare-earth-doped optical fibers," Opt. Express **29**, 40345-40359 (2021).
[66] Huang, D., Tran, M. A., Guo, J., Peters, J., Komljenovic, T., Malik, A., Morton, P. A., and Bowers, J. E., "High-power sub-khz linewidth lasers fully integrated on silicon," Optica **6**, 745-752 (2019).
[67] Preda, C. E., Fotiadi, A. A., and Megret, P., "Numerical approximation for brillouin fiber ring resonator," Opt Express **20**, 5783-5788 (2012).
[68] Grukh, D. A., Kurkov, A. S., Razdobreev, I. M., and Fotiadi, A. A., "Self-q-switched ytterbium-doped cladding-pumped fibre laser," Quantum electronics **32**, 1017 (2002).
[69] Morrison, B., Casas-Bedoya, A., Ren, G., Vu, K., Liu, Y., Zarifi, A., Nguyen, T. G., Choi, D.-Y., Marpaung, D., Madden, S. J., Mitchell, A., and Eggleton, B. J., "Compact brillouin devices through hybrid integration on silicon," Optica **4**, 847-854 (2017).